Int. J. Multiphase Flow Vol. 17, No. 4, pp. 439–454, 1991
Printed in Great Britain.

0301-9322/91 $3.00 + 0.00

PROPERTIES OF THE LIQUID LAYER IN HORIZONTAL ANNULAR FLOW

S. V. PARAS and A. J. KARABELAS

Department of Chemical Engineering, University of Thessaloniki and Chemical Process Engineering Research Institute, P.O. Box 1517, 540 06 Thessaloniki, Greece

(Received 15 August 1990; in revised form 20 February 1991)

Abstract—Time records have been collected of local liquid film thickness, using parallel-wire conductance probes, in a new 50.8 mm i.d. pipe loop. Statistical analysis of these records allows the study of the circumferential variation of time-averaged thickness, of RMS values and of other quantities. The power spectra show that the dominant frequency associated with large disturbance waves is < 10 Hz at low gas velocities, displaying a tendency to increase with gas flow rate. By combining signal cross-correlation data with visual observations, it is shown that the disturbance waves tend to deform rapidly, move on a plane inclined with respect to the vertical and cover an increasingly larger portion of the circumference with increasing gas velocity. The mean large wave height at the pipe bottom is linearly related to the local RMS value. It is also a strong function of gas flow rate, with a moderate dependence on liquid flow rate. The wave steepness shows a similarly strong dependence on gas flow rate. However, the disturbance wave intermittency appears to be almost independent of gas as well as liquid flow rates.

Key Words: gas–liquid flow, annular flow, film properties, disturbance waves

1. INTRODUCTION

Considerable work has been carried out over the past 30 years on horizontal annular flow. Yet many important questions remain unanswered. Perhaps the most significant issue concerns the dominant mechanism for transport of liquid from the bottom part of the pipe to the top, necessary for a continually wetted pipe surface. Evidently, *droplet entrainment* (mostly from the lower part of the pipe) and *redeposition* contribute to the formation of the liquid layer at the top. Anderson & Russell (1970) present experimental results from a 25.4 mm i.d. pipeline on the rate of droplet deposition and its circumferential variation. Using these results, and his own film thickness measurements, Butterworth (1972) argues that the magnitude of droplet deposition rates is insufficient to sustain the film at the upper part of the pipe. On the contrary, James *et al.* (1987) in their modeling effort consider the entrainment/deposition mechanism to be of primary importance. By adjusting a parameter characterizing this mechanism, they obtain a good fit with measured circumferential film thickness distributions.

Other proposed mechanisms are attributed to the complicated gas–liquid wave interactions. Pletcher & McManus (1965) consider that the circumferential variation of film thickness and roughness can induce a two-vortex *secondary flow* in the gas phase. The resulting circumferential shear stress at the interface can drive liquid in a direction opposite to gravity. There is no direct experimental evidence supporting this mechanism, other than the measurements taken by Darling & McManus (1968), for *single-phase* gas flow in an eccentrically threaded pipe, which confirm the existence of secondary flow. In recent modeling efforts, Laurinat *et al.* (1984) and Lin *et al.* (1985) take into account the secondary flow mechanism and the related circumferential interfacial stresses. Laurinat *et al.* (1984) conclude that these stresses, as well as normal stresses (due to circumferential fluctuations in the film) are primarily responsible for moving liquid to the upper part of the pipe. Lin *et al.* (1985) propose that both the secondary flow and the entrainment/deposition mechanisms are important. By adjusting various parameters in these models, again good agreement is obtained between predicted and measured film thickness distributions.

Butterworth (1972) suggests a *wave spreading mechanism* to interpret his observations. Waves at the lower part of the pipe are considered to be deformed, with the front (right at the bottom) moving faster. The impact pressure of the gas on such a wave can give rise to forces acting in the circumferential direction, which can then transfer liquid in that direction against gravity.

Fukano & Ousaka (1989) model liquid transfer to the top by assuming a *pumping action* due to disturbance waves. By considering that these waves have a circumferentially varying amplitude (with the maximum at the bottom), a corresponding static pressure variation is assumed along the waves due to the faster moving gas. Thus, a negative pressure gradient may exist, resulting in a pumping action of liquid towards the upper part of the pipe. Fukano & Ousaka (1989) claim that their model predictions are in better agreement with measured film distributions than those obtained by Laurinat *et al.* (1985).

It is clear from the above brief review that the accurate description of liquid film properties is essential in understanding the mechanics of horizontal annular flow. Detailed experimental data on film properties are very limited. The papers by Sekoguchi *et al.* (1982) and Fukano *et al.* (1983) appear to be the only experimental studies, carried out in a 26 mm i.d. pipe, where statistical liquid film characteristics are reported. Hanratty and his coworkers (Dallman, 1978; Laurinat, 1982; Williams, 1986) have studied various aspects of horizontal annular flow in pipelines of 23, 50 and 95 mm i.d., but no detailed analysis of time records has been presented so far. Butterworth & Pulling (1973), Fisher & Pearce (1978) and Lin *et al.* (1985) have presented data on film thickness distribution obtained in a limited number of experiments. Finally, when this work was completed the study by Jayanti & Hewitt (1990) was brought to our attention. This study was carried out in a 5.5 m long pipeline of 32 mm i.d. and statistical techniques were used to analyze film thickness records measured by conductance probes.

The experimental work reported so far in the literature has shed some light on the effect of gravity on the asymmetric film distribution. However, only fragmented information is available on other liquid film characteristics and, in particular, on the properties of large disturbance waves.

The work reported here is part of a study aimed at clarifying the basic characteristics of horizontal annular flow. For this purpose a new pipe loop of 50.8 mm i.d. was constructed. In the paper a description of the experimental equipment and procedures are presented first. Detailed data analysis and interpretation is given in the next section. New information is presented on the circumferential variation of the film thickness standard deviation and on the frequency spectra of film thickness fluctuations. To accurately describe disturbance waves, various properties have been extracted from the film thickness time records; they include wave celerity, height, length, width, intermittency and steepness. These data, complemented with visual observations, shed new light on the complicated gas–liquid film interactions. They are also employed to interpret droplet flux measurements, presented in the companion paper (Paras & Karabelas, 1991, this issue, pp. 455–468).

2. EXPERIMENTAL EQUIPMENT AND PROCEDURES

2.1. Flow loop

The experiments were conducted in a horizontal two-phase flow loop which is illustrated in figure 1. The pipeline consists of a 16 m long, 5.08 cm i.d., straight pipe section and a 180° 5.08 cm i.d. bend, followed by an 8 cm i.d. pipe having a length of 16 m. The 5.08 cm i.d. pipe consists of two parts, a 9 m stainless-steel (SS) part and a 7 m transparent Plexiglas part, to facilitate visual observations. The pipelines are made of flanged sections to allow the insertion and removal of experimental test sections at various locations. The mixing section for the two phases is a simple tee with the liquid phase introduced in the branch and the gas phase in the run. The distance between the mixing section and the test section is ≈ 15 m, i.e. approx. 300 pipe diameters, considered sufficient for fully developed flow.

In order to minimize flow disturbances due to a possible mismatch between pipe joints, tongues and grooves were machined into the flanges of adjacent pipe sections. Additionally, the inside pipe walls were machined to a 3° taper at the end of the sections. Sealing was provided by the use of O-rings in such a way that the flange faces would fit almost perfectly.

Careful attention was paid to aligning the pipeline with the use of metal supports at about 1.35 m intervals. Due to the sensitivity of the flow regime transition to pipeline inclination (Barnea *et al.*, 1980), the pipeline was carefully leveled. Horizontal alignment was achieved by using a plumb line. Finally, to check the staightness of the pipe, a laser beam was placed inside one end of the pipeline and sighted at the other end.

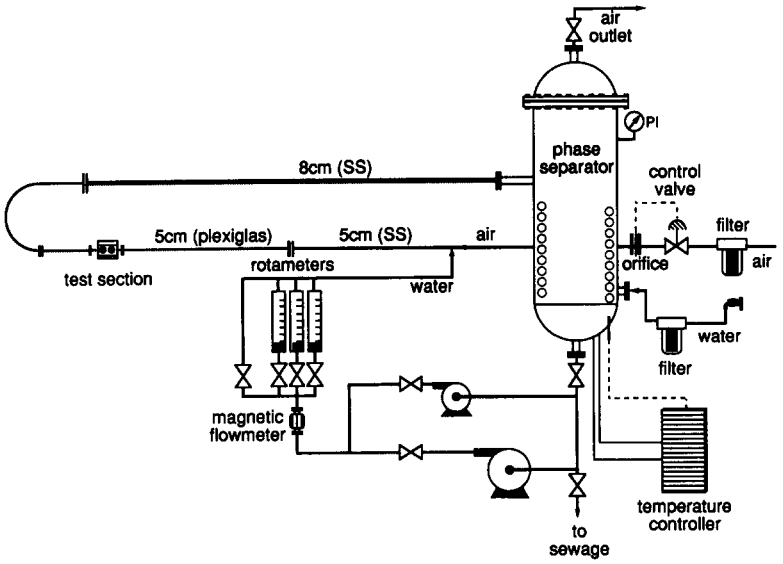

Figure 1. Experimental setup for two-phase flow measurements.

The flow at the end of the return pipe enters tangentially, through a 5 cm entrance section, a 1.8 × 0.6 m dia cylindrical phase separator. The separator was constructed using 2.5 mm SS-304 plate. A cooling coil, made of 2.5 cm SS pipe and 35 m in length, is installed in the lower part of the separator and is connected to a refrigeration system, in order to keep the temperature of the recirculating water under control.

The air from the separator is vented to the atmosphere through an 8 cm gate valve, which controls the discharge pressure. Droplets are removed from the air by a demister located at the exit of the separator. The water is either discharged to the laboratory sewage system or recycled back to the flow loop through a system of pumps. Water may be supplied to the separator tank from a municipal water line after it is passed through a system of water filters (1 μm final pore size). Two SS centrifugal pumps are used delivering 30 m^3/h at 2 atm and 2 m^3/h at 1.5 atm, respectively.

The water flow rate is measured using a bank of three rotameters, each covering part of the range of flow rates (max. 0.4, 1.2, 2.6 m^3/h). A 32 mm i.d. magnetic flow meter is also employed for high flow rates (up to 15 m^3/h), especially for single-phase flow during the calibration of various measuring devices. The accuracy of the rotameters and of the magnetic flowmeter is better than $\pm 1\%$.

Air supplied by two compressors with a total capacity of 15 m^3/min at 1 atm (working pressure 7 atm), passes through a 2 m^3 pressurized vessel, a dryer, a cooler, filters and a pressure regulator. The air flow rate is controlled with a pneumatic control valve and is measured by an orifice plate with an accuracy of $\pm 5\%$.

A flow regime map was constructed for air–water flow in the 5.08 cm pipe, based on approx. 100 observations under various flow conditions. The location of the observation area was 260 dia downstream of the mixing section of the pipe loop. The boundaries between the flow regimes for air–water flow in the 2.5 and 10 cm pipe presented by Lin (1985) are superimposed on our results for comparison (figure 2). A relatively close agreement is observed between flow regime boundaries for 5 and 10 cm i.d. pipes.

2.2. Experimental techniques

Wave heights and liquid film thickness along the pipe in two-phase flow are measured using parallel-wire conductance probes. This measuring techniques relies on the fact that the conductance between two parallel wires is uniquely related to the liquid level between them. The parallel-wire probes require an electronic analyzer circuit (Andritsos 1986), which measures the conductance of the liquid film between the wires and produces a d.c. output corresponding to the film height.

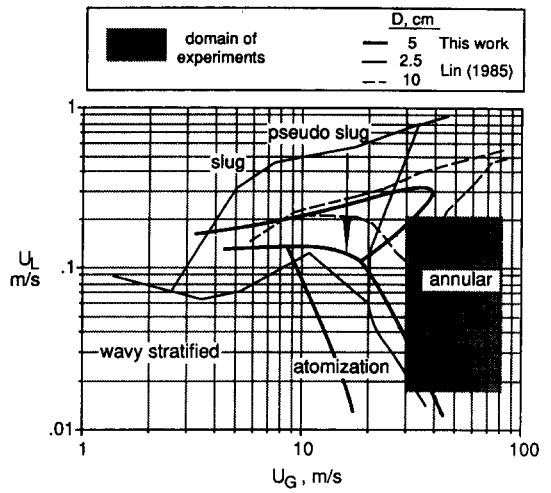

Figure 2. Flow regime map for horizontal two-phase flow (air–water in a 5.08 cm i.d. pipe) and comparison with flow regime observations by Lin (1985).

A Plexiglas test section was designed and constructed for film thickness measurements. The probes were in the form of cylindrical plugs which could be inserted into the test section. The plugs were machined so that they were flush with the inside pipe wall when mounted onto the test section. Each probe had two parallel chromel wires 0.5 mm dia, 2.5 mm apart with a 12 mm length exposed to flow. The two wires were embedded almost radially on the same pipe cross section. A total of 8 probes, spaced at 45° intervals, could be placed around the circumference of the pipe. A second set of 8 probes could be located 6 cm upstream of the first set for performing wave celerity measurements. Three probes were fabricated with the intention to use them simultaneously. However, in preliminary tests an interaction of the electric fields of two neighboring probes was noticed, resulting in a reduction of the signal. Therefore, only one probe at a time was used to obtain film thickness data. Two- and three-probe measurements were performed simultaneously only in cases where a small signal reduction was of no consequence, e.g. for cross-correlation and comparison of film traces.

The effect of temperature on the water conductivity was eliminated by measuring the conductivity before and after each run and by incorporating a correction factor in the voltage to film thickness conversion. The accuracy of the measurements throughout the range covered is around $\pm 5\%$, taking into account uncertainties in the calibration procedure (i.e. temperature variations). The technique is considered inadequate for film thickness < 0.05 mm. Details on the probe accuracy and the calibration procedure are reported by Karapantsios *et al.* (1989).

Measurements were taken at six circumferential positions, i.e. at the bottom ($\Theta = 0°$), at 45°, 90°, 135°, 180° and 315° from the bottom of the pipe. Initially, the three probes were located at 0°, 90° and 180°. Rotating the test section by 45°, the probes were placed at 45°, 135° and 315° respectively. Data of time-averaged thickness h at 45° and 315°, collected to check the symmetry of the liquid film with respect to the vertical plane, reveal a great degree of symmetry. The range of superficial velocities covered in the tests, was $U_L = 1.9$ to 20 cm/s for water and $U_G = 31$ to 66 m/s for air, which correspond to annular two-phase flow as shown in figure 2.

2.3. Methods of data acquisition and analysis

Analog signals from film thickness analyzers were digitized and stored for subsequent analysis. Analog-to-digital conversion was performed by a 12-bit, 16-channel A/D converter and data obtained were transferred to a Macintosh Plus (1 Mb) microcomputer for storage and analysis. Each data set was collected for a period of 16.5 s with a sampling frequency of 250 Hz. Data for wave celerity calculations were sampled with a sampling frequency of 1000 Hz. The digitized voltage signal was converted to film height by means of a calibration curve. The local *time-averaged* liquid film thickness h is necessary in order to obtain the mean film thickness throughout the pipe

Table 1. Summary of experimental conditions and results

Run	U_L (m/s)	U_G (m/s)	ρ_G (kg/m^3)	W_L (kg/s)	W_G (kg/s)	$\langle h \rangle$ (mm)	$\langle$RMS$\rangle$ (mm)	ϵ (%)	U_{LF} (m/s)
A	0.03	31.1	1.27	0.06	0.08	0.35	0.15	2.8	0.95
B	0.03	38.1	1.52	0.06	0.11	0.27	0.09	2.2	0.98
C	0.03	49.4	1.67	0.06	0.16	0.20	0.05	1.5	1.00
D	0.06	31.6	1.39	0.12	0.09	0.47	0.22	3.7	1.36
E	0.06	43.0	1.66	0.12	0.14	0.30	0.11	2.3	1.39
F	0.06	48.0	1.78	0.12	0.17	0.23	0.08	1.8	1.22
G	0.09	32.5	1.58	0.18	0.10	0.58	0.24	4.6	1.57
H	0.09	46.5	1.91	0.18	0.17	0.25	0.09	2.0	1.70
I	0.12	30.1	1.55	0.25	0.09	0.74	0.32	5.8	1.76
J	0.12	45.4	2.00	0.25	0.18	0.30	0.11	2.3	1.28
K	0.02	65.5	1.98	0.04	0.26	0.08	0.02	0.6	1.85
L	0.02	49.6	1.63	0.04	0.16	0.13	0.03	1.0	1.25
M	0.02	32.2	1.40	0.04	0.09	0.22	0.10	1.8	0.94
N	0.03	65.5	2.19	0.06	0.28	0.09	0.02	0.7	1.88
O	0.20	46.8	2.31	0.39	0.21	0.31	0.14	2.4	2.35
P	0.20	31.7	1.65	0.39	0.10	0.84	0.33	6.6	2.34
Q	0.06	61.5	2.33	0.12	0.28	0.10	0.03	0.8	2.32

cross section $\langle h \rangle$, which is calculated by integrating data such as those of figure 5, covering only one-half of the pipe perimeter.

The root-mean-square (RMS) values and the power spectral density (PSD) of the film thickness fluctuations were computed in order to characterize the wavy gas–liquid interface and to facilitate modeling gas–liquid transport processes, including interface friction (pressure drop) and liquid atomization. Signal cross-correlation was employed to specify the celerity of waves traveling on the film. Special software was developed for the analysis of the above quantities, which are defined as in Bendat & Piersol (1971).

Experimental conditions and some of the measured quantities are summarized in table 1. U_L and U_G are the superficial liquid and gas velocities, W_L and W_G are the mass flow rates, ρ_G is the gas

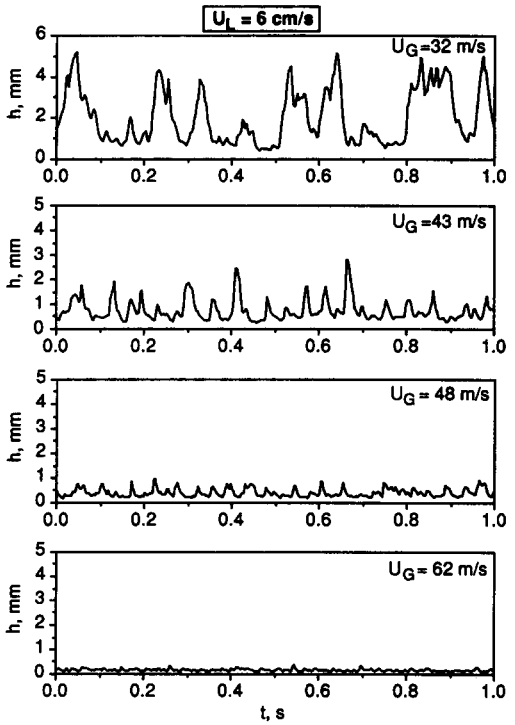

Figure 3. Typical traces at the pipe bottom ($\Theta = 0°$) for a fixed superficial liquid velocity ($U_L = 6$ cm/s).

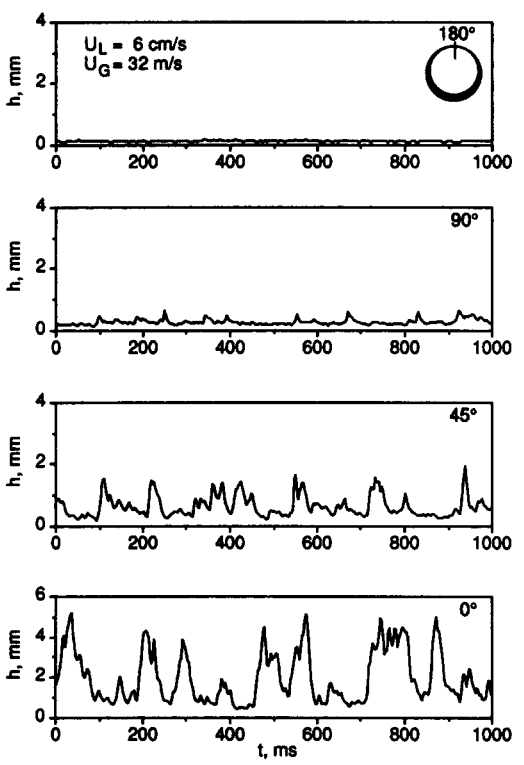

Figure 4. Typical traces at various angular positions for low superficial gas velocity ($U_L = 6$ cm/s, $U_G = 32$ m/s).

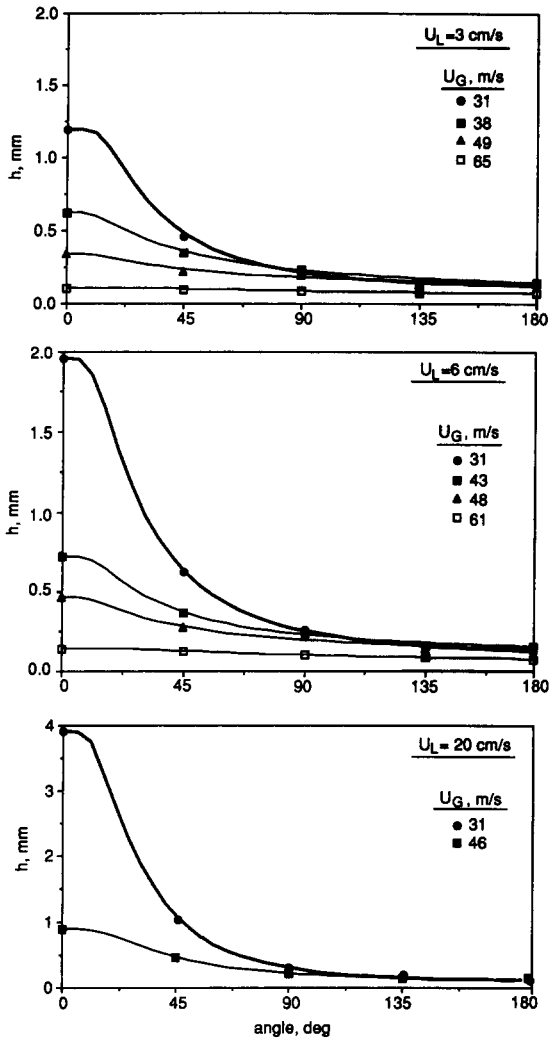

Figure 5. Film thickness distribution around the pipe circumference.

density, ϵ is the liquid film holdup, U_{LF} is the mean film velocity, and $\langle\ \rangle$ refers to quantities averaged throughout the pipe cross section.

3. DATA ANALYSIS AND INTERPRETATION

3.1. Film thickness and RMS circumferential distribution

Typical traces corresponding to the pipe bottom ($\Theta = 0°$), for a fixed superficial liquid velocity, are shown in figure 3. The dramatic reduction of liquid film thickness with increasing superficial gas velocity is evident. Moreover, the amplitude of waves is greater at small gas flow rates. The traces in figure 4 depict the influence of gravity on liquid distribution in the pipe circumference at a relatively small gas velocity. The drastic reduction of the gas–film interface roughness in the circumferential direction is expected to play a major role in mass and momentum interchange, as has been also pointed out in previous studies.

Representative data sets are plotted in figure 5, showing the (time-averaged) film thickness distribution around the pipe circumference. The solid lines are interpolating curves based on a general formula originally proposed by Sekoguchi *et al.* (1982). The good fit, obtained by adjusting two parameters, is necessary for integrating each profile to compute the average thickness $\langle h \rangle$.

For low gas flow rates ($U_G < 40$ m/s) and for all liquid rates tested, the film is highly asymmetric due to gravity. As the gas flow rate increases, the liquid film height, as well as the rest of its properties, tend to be distributed uniformly around the pipe circumference, implying that the role

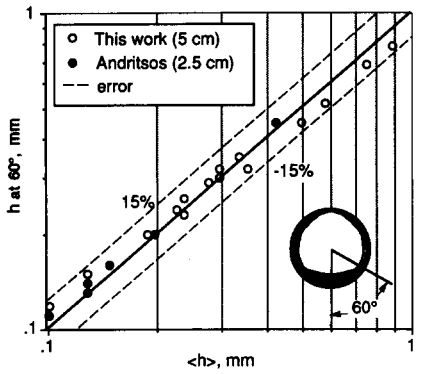

Figure 6. The local film thickness at 60° is nearly equal to the global average $\langle h \rangle$.

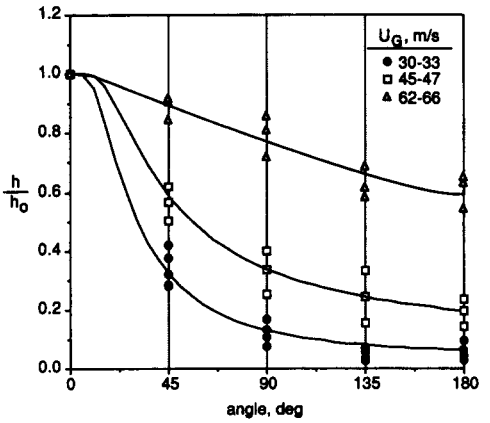

Figure 7. Film thickness distribution normalized with respect to thickness at $\Theta = 0°$. Correspondence of symbols with runs (table 1): ● A, I, D, P, M.: □ J, H, O; △ Q, K, N.

of gravity is almost negligible under these conditions. For instance, at $U_G > 50$ m/s the value at the top of the pipe is almost 80% of the value at the bottom.

In general, the average film thickness $\langle h \rangle$ data tend to follow a correlation proposed by Laurinat *et al.* (1984), although the latter underpredicts $\langle h \rangle$ as compared with the measurements. On the contrary, the data by Williams (1986), obtained in a 10 cm pipe, fall below the correlation. It is, therefore, possible that the effect of diameter is not properly taken into account.

It is of interest to point out here that the local film thickness at a *specific* circumferential location is, for practical purposes, equal to the global average $\langle h \rangle$. This location is for our experiments approx. 60° from the pipe bottom. Figure 6 shows that this is, indeed, a satisfactory approximation for our data as well as those of Andritsos (1986) obtained in a 25 mm i.d. pipe. Sekoguchi *et al.* (1982) also report a similar characteristic value ($\Theta \approx 60°$) for their data obtained in a 26 mm i.d. pipe. However, the characteristic value for large diameter pipes appears to be smaller.

Another interesting result is obtained from our data by normalizing the local time-averaged film thickness profiles with respect to the value at the bottom ($\Theta = 0°$). As shown in figure 7, the normalized profiles appear to be influenced by gas velocity only, the effect of liquid flow rate being insignificant. This observation could be useful in future modeling efforts, if it is proven to hold under different conditions as well.

Typical circumferential profiles of RMS film thickness fluctuations are presented in figure 8. There is a strong effect of liquid flow rate on the RMS values, especially in the lower half of the pipe. Otherwise, the RMS profiles exhibit the same trends as the film thickness h, with regard to gas velocity and gravity effects.

The *intensity* of film thickness fluctuations is defined as RMS/h, where h and RMS are the local values of the time-averaged film thickness and its standard deviation, respectively. Figure 9 shows that the highest values of intensity are observed at low gas and high liquid flow rates. At high gas flow rates the intensity of h fluctuations is almost symmetric around the pipe circumference with a value of 0.2–0.3, whereas at low gas rates it is very asymmetric with the highest values in the lower half of the pipe. It will be noted that for low gas velocities ($U_G = 30$ m/s) and relatively high liquid velocities ($U_L > 6$ m/s) the intensity RMS/h attains its maximum value at $\Theta \approx 45°$ rather than at $\Theta = 0°$, where the maximum for all other cases is observed.

3.2. *Wave frequency and celerity*

The power spectral density (PSD) of the film height time series have been obtained by averaging modified periodograms, as reported by Paras & Karabelas (1990). According to Bendat & Piersol (1971) the resulting standard error on the final estimate is 11%, which is plotted as error bars on the power spectra.

Figure 10a shows power spectra of film thickness fluctuations corresponding to a relatively low gas velocity. There is no influence of liquid velocity on the form of the spectra. However, the

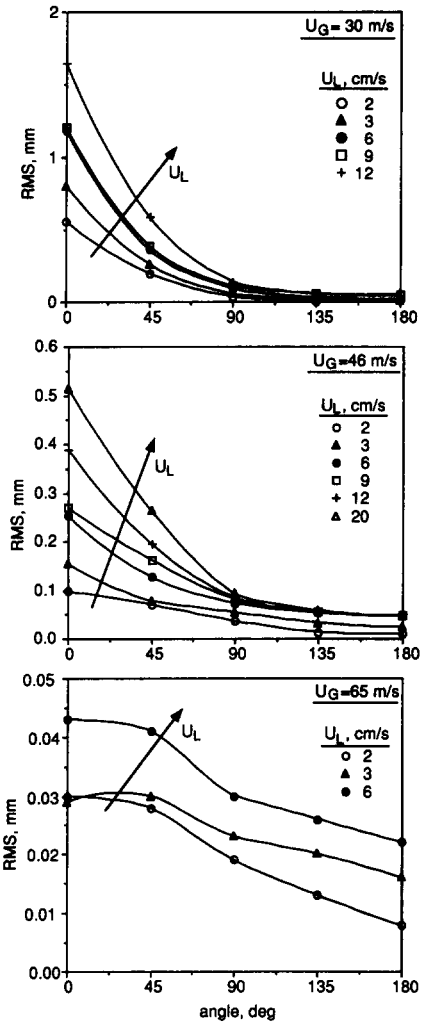

Figure 8. Distribution of RMS values of film thickness fluctuations.

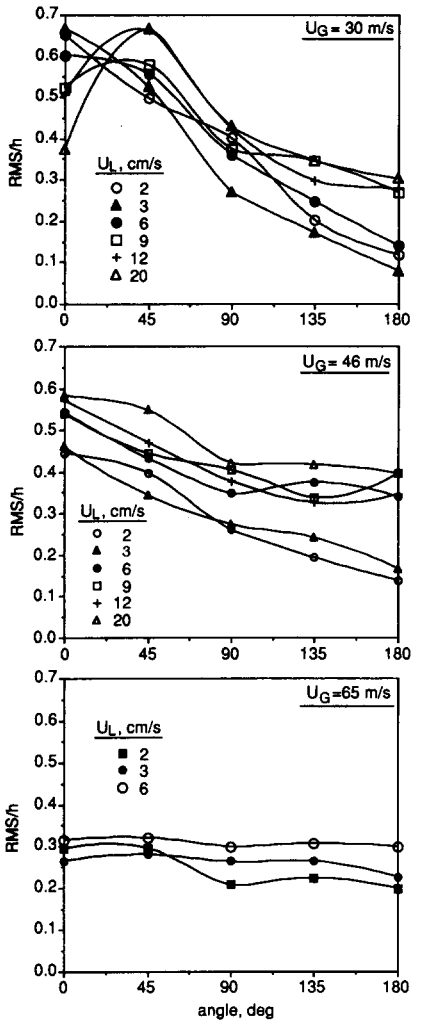

Figure 9. Distribution of intensity of film thickness fluctuations.

dominant frequency appears to decrease with increasing liquid flow rate. Under the above conditions, a large portion of wave energy at the pipe bottom is carried by waves of frequency < 10 Hz. Figure 10b shows that, for a fixed liquid rate, increasing the gas flow rate tends to distribute the energy to waves of higher frequency. Moreover, the spectrum tends to flatten out with increasing U_G, due to the more uniform distribution of energy among waves of a broad frequency range.

Figure 11 shows power spectra of film thickness at three locations in the pipe circumference ($\Theta = 0°$, 45° and 90°) for relatively small gas and liquid flow rates. The amplitude of the spectrum decreases by several orders of magnitude between the pipe bottom and a location $\Theta = 90°$. The measured drastic reduction of film thickness in the circumferential direction is in accord with the above trend. It will also be noted in figure 11 that there is no appreciable change of the dominant frequency in these spectra.

In order to interpret the dominant frequency of the spectra and to obtain additional information on the wave structure, visual observations were made in the Plexiglas section of the flow loop. The observations were made by using light pulses of a frequency close to the dominant frequency of each spectrum. Thus, the waves on the film could be "frozen" to facilitate the observations. Under these conditions, "ring-shaped" wave structures were observed covering a large portion of the pipe circumference. For small gas velocities ($U_G < 40$ m/s) these ring-shaped waves covered the lower half of the pipe and moved, at an angle with respect to the pipe cross section, with their front at the bottom. With increasing gas flow rate, the waves appeared to cover a larger portion of the

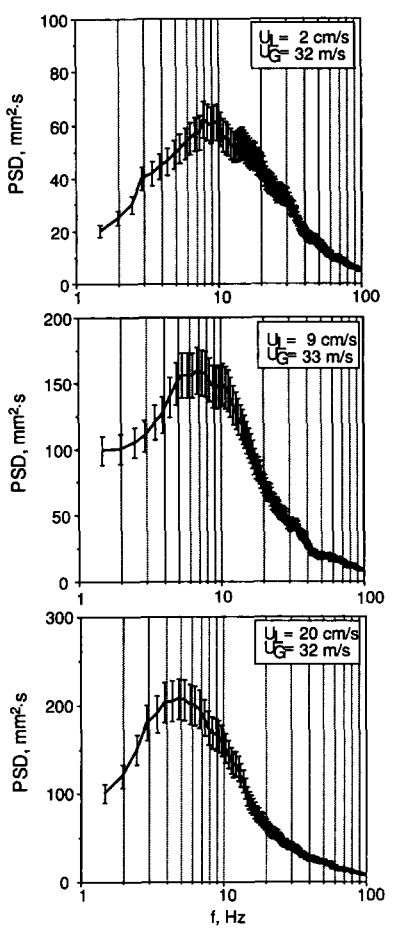

Figure 10a. PSD of film thickness fluctuations for low gas flow rate (at $\Theta = 0°$).

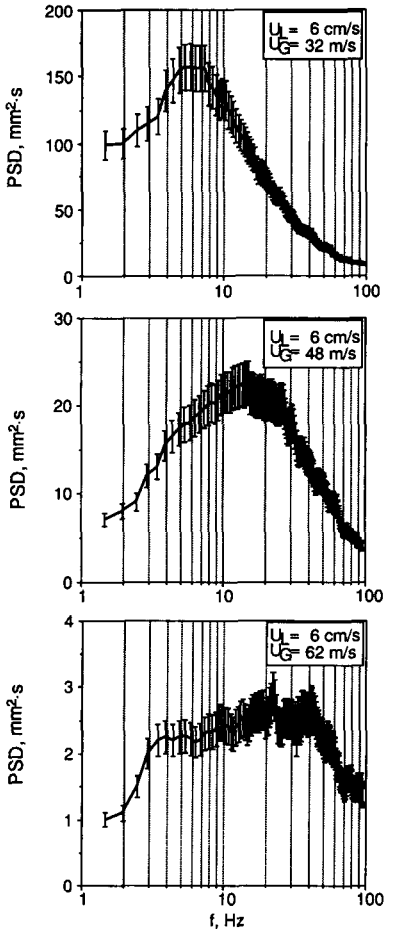

Figure 10b. PSD of film thickness fluctuations for a fixed superficial liquid velocity ($U_L = 6$ cm/s) at various superficial gas velocities ($\Theta = 0°$).

circumference while their characteristic angle was gradually reduced to zero. These are obviously the large disturbance waves often quoted in the literature. The photograph in figure 12 shows such a wave.

The above visual observations are verified by computing the cross-correlation function of signals from two probes positioned at $\Theta = 0°$ and 90°. By selecting the time delay which corresponds to the best correlation of the cross-correlation function, and assuming a constant wave celerity throughout the pipe circumference, the angle of wave inclination is specified. Figure 13 presents this interesting information as a function of U_G. It is clear that only at high gas velocities ($U_G > 50$ m/s) does the angle of the disturbance waves tend to become zero. As has been observed elsewhere (Paras & Karabelas 1990), at small U_G and relatively high U_L values a better correlation is obtained between signals at $\Theta = 0°$ and 90°, suggesting a greater coherence of the ring-shaped waves under these conditions.

Celerities of large waves, moving at the lower part of a pipe, are obtained by calculating the cross-correlation function of two simultaneously recorded signals from locations at a distance $\Delta x = 6$ cm and $\Theta = 0°$. The celerity $U_c = (\Delta x/\Delta t)$ is computed by determining the time delay Δt which corresponds to the best correlation between the two signals. Figure 14 presents the celerities, which are associated with the large disturbance waves. The systematic increase of U_c with increasing gas and liquid velocities is very clear. A comparison is made in figure 15 of celerities determined in this study with those obtained by Fukano *et al.* (1983), under the same superficial velocities U_G and U_L, but in a 26 mm i.d. pipe. Although the trend in both sets of data is the same, the smaller diameter pipe is associated with higher celerities.

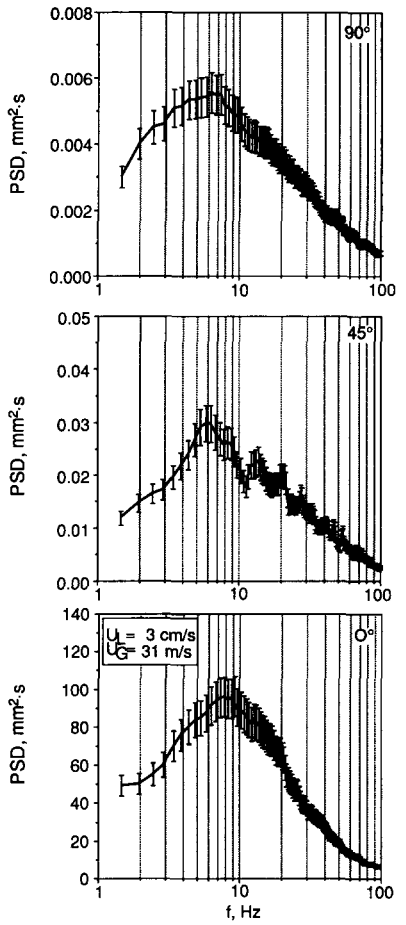

Figure 11. PSD of film height fluctuations at $\Theta = 0°$, 45° and 90° ($U_L = 3$ cm/s, $U_G = 31$ m/s).

3.3 Geometric characteristics of large disturbance waves

The evidence presented so far clearly suggests that the wave structure is dominated by the large disturbance waves. At relatively small gas flow rates, where gravity is important, these waves are

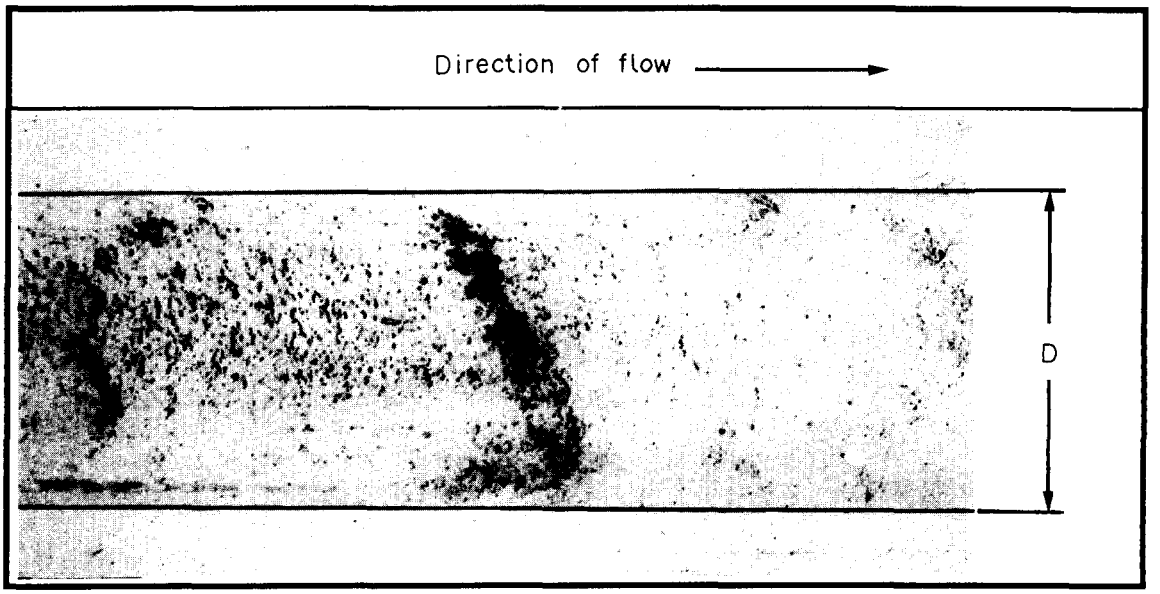

Figure 12. Disturbance waves in annular air–water flow ($U_G = 50$ m/s, $U_L = 6$ cm/s).

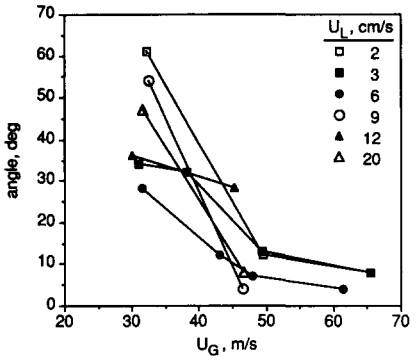

Figure 13. Influence of superficial liquid and gas velocities on disturbance wave deviation from the vertical.

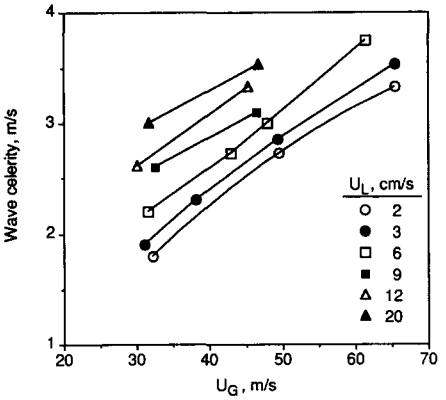

Figure 14. Influence of superficial liquid and gas velocities on disturbance wave celerity (at $\Theta = 0°$).

more pronounced at the pipe bottom. With increasing gas flow rate, they tend to be distributed uniformly around the circumference. Therefore, the best location to study the large wave characteristics, for all flow rates examined in this work, is the pipe bottom ($\Theta = 0°$). The results presented here on large-disturbance-wave height, width, length, intermittency and steepness correspond to this location. Figure 16 is used to define the above properties. Results relating to large disturbance waves at the pipe bottom are summarized in table 2.

The wave height h_w is measured from the pipe surface. Wave intermittency, defined as the fraction of total sampling time corresponding to the passage of large disturbance waves, is useful in the description of processes taking place at the gas–liquid interface (Schadel 1988). This quantity is not easily extracted from the data as it is difficult to unequivocally determine the required geometric wave properties such as amplitude, width etc.

Nencini & Andreussi (1983) define the wave amplitude as one-half the height difference Δh between a minimum in the film trace and the subsequent maximum. Schadel (1988) has proposed a procedure to compute large wave width and intermittency. The dominant frequency obtained from the spectra is employed as a criterion for selecting the large waves. Additionally, the wave width is defined as the distance between two successive minima of the film thickness record. However, in the case of a large wave with ripples riding on it, this procedure discards the part of the wave width following the minimum of the first ripple, leading to an underestimation of the true width and, consequently, of the intermittency. A modification of the above procedure was introduced in our computer program to improve these estimates, by adding the width of all the small disturbances to the width of the preceding large disturbance wave. The length of large waves, λ, is defined as the distance between the peaks of two such successive waves. It can also be computed as follows:

$$\lambda = U_c/f,$$

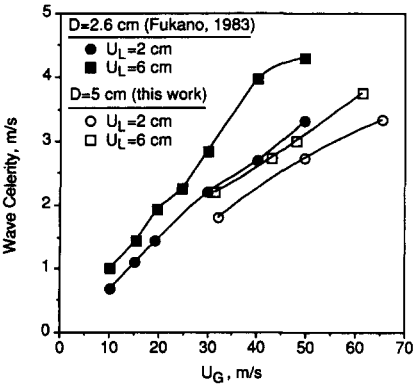

Figure 15. Comparison of celerities determined in this study with those obtained by Fukano *et al.* (1983).

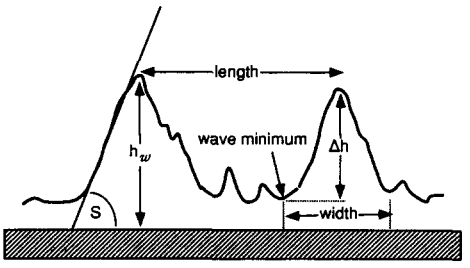

Figure 16. Definition of disturbance wave characteristics.

Table 2. Summary of results at $\Theta = 0°$ (pipe bottom)

Run	h_0 (mm)	RMS_0 (mm)	U_c (m/s)	h_w (mm)	Width (mm)	Length (mm)	f (Hz)	I
A	1.20	0.80	1.90	3.09	83	238	8	0.38
B	0.62	0.38	2.22	1.56	79	202	11	0.38
C	0.34	0.15	2.86	0.73	83	191	15	0.43
D	1.95	1.18	2.20	4.35	103	314	7	0.35
E	0.72	0.43	2.73	1.80	100	273	10	0.37
F	0.46	0.25	3.00	1.06	86	200	15	0.42
G	2.31	1.21	2.60	4.48	152	433	6	0.35
H	0.50	0.27	3.10	1.14	90	238	13	0.38
I	3.24	1.64	2.61	5.71	173	522	5	0.34
J	0.68	0.39	3.33	1.59	118	333	10	0.35
K	0.10	0.03	3.33	0.17	65	167	20	0.39
L	0.22	0.10	2.73	0.46	77	182	15	0.42
M	0.85	0.55	1.80	2.41	65	200	9	0.35
N	0.11	0.03	3.53	0.17	67	141	25	0.48
O	0.89	0.51	3.53	2.05	152	504	7	0.31
P	3.90	1.46	3.00	5.77	186	600	5	0.30
Q	0.14	0.04	3.75	0.23	75	170	22	0.43

where U_c is the wave celerity and f the corresponding frequency. Using this modified procedure, mean values for large-wave height, width, length and intermittency have been obtained.

The mean *large-wave height* (h_w) at the pipe bottom ($\Theta = 0°$) is found to be a linear function of the RMS value of the film height at $\Theta = 0°$; i.e. $h_w = 4\,(RMS_0)$. Moreover, it is very interesting that data on the mean height difference Δh can be related to RMS_0 as follows:

$$\Delta h = 2\sqrt{2}\,(RMS)_0$$

with an error $< \pm 15\%$ (figure 17). It will be recalled at this formula is accurate in the case of sinusoidal waves of amplitude $\Delta h/2$.

The gas flow rate has a strong influence on the large-wave height, as shown in figure 18. The effect of superficial liquid velocity on the large-wave height is significant only at relatively low gas flow rates; i.e. for $U_G < 50$ m/s. The RMS values at the bottom display the same trends, which explains the linearity between RMS_0 and h_w. This also implies that the large waves are mainly responsible for the magnitude of the RMS of the fluctuating liquid layer.

The mean *large-wave width* is well-correlated with the corresponding wavelength, being approx. 35% of the latter for all our experiments. This nearly constant ratio can be explained, by observing that (with increasing gas flow rate) a decrease of the wave width is accompanied by a reduction of the wavelength due to the increase of the large-wave frequency.

Intermittency values of large disturbance waves, computed as outlined previously, are plotted in figure 19 as a function of superficial gas velocity. The influence of gas and liquid flow rates is evidently insignificant, as most of the computed intermittency values vary in the narrow range 0.35–0.45. A possible small effect of the gas velocity is masked by the spread of the data points. The roughly constant intermittency values are in accord with the nearly constant ratio of wave

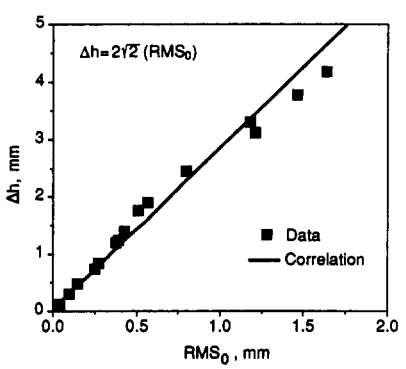

Figure 17. Mean height different Δh relation to the corresponding RMS_0 (at $\Theta = 0°$).

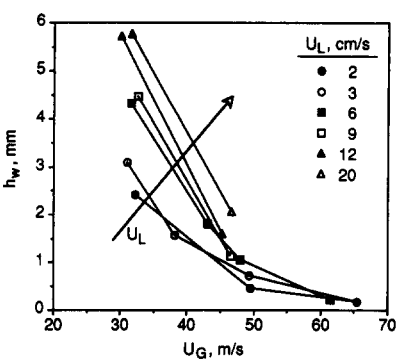

Figure 18. Influence of superficial liquid and gas velocities on disturbance wave height (at $\Theta = 0°$).

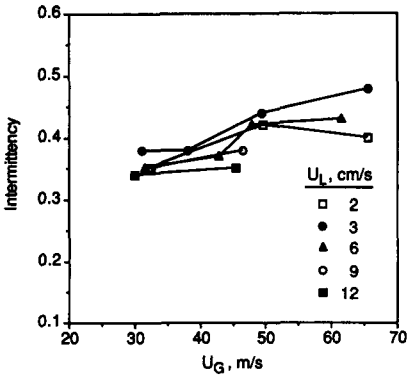

Figure 19. Influence of superficial liquid and gas velocities on disturbance wave intermittency (at $\Theta = 0°$).

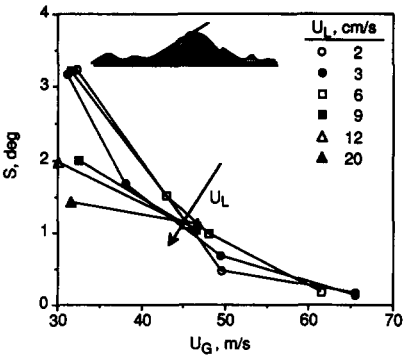

Figure 20. Influence of superficial liquid and gas velocities on disturbance wave steepness (at $\Theta = 0°$).

width to wavelength. It must be also noted that this ratio is, by definition, equivalent to intermittency.

A useful geometric parameter, describing the shape of large waves, is the wave steepness S. It is defined as

$$S = \arctan(0.5\Delta L/\Delta h),$$

where ΔL and Δh can be substituted by the mean large-wave width and twice the mean wave amplitude, respectively. The data show that the steepness tends to increase with decreasing U_G and U_L (figure 20), but it is a rather strong function of U_G and a weak function of U_L. Moreover, it is noticed that, unlike the large-wave height, the steepness has a tendency to decrease with increasing liquid flow rate.

4. CONCLUDING REMARKS

The data clearly show the influence of gravity at relatively low gas flow rates. Of particular significance are the relatively high values of RMS and of the intensity of film thickness fluctuations (RMS/h) in the lower part of the pipe. These high values do not support the assumption, made in modeling efforts (e.g. Laurinat *et al.* 1985), that the temporal variations of h are not very significant. The non-uniform distribution of RMS values is expected to play a major role in momentum interchange processes, thus influencing interfacial friction and atomization, as discussed by Paras & Karabelas (1991).

The dominant frequencies of the power spectra display the strong effect of gas flow rate. By making visual observations, it was established that the dominant frequency corresponds to *large disturbance waves*, covering an increasingly large portion of the circumference with increasing U_G. These larger waves appear to be on a plane (moving with a constant wave celerity U_c) which is inclined with respect to the pipe cross section (figure 12). The respective angle of inclination tends to zero with increasing U_G (figure 13).

Table 3. Additional large wave celerity data

				$\Delta x = 3$ cm		$\Delta x = 9$ cm		$\Delta x = 12$ cm	
Run	U_L (m/s)	U_G (m/s)	U_c (m/s)	U_c (m/s)	Corr. coeff.	U_c (m/s)	Corr. coeff.	U_c (m/s)	Corr. coeff.
B	0.03	38.1	2.22	2.50	0.86	2.50	0.68	2.50	0.64
C	0.03	49.4	2.86	3.00	0.85	3.00	0.64	3.08	0.56
D	0.06	31.6	2.20	2.20	0.93	2.18	0.85	2.18	0.79
E	0.06	43.0	2.73	3.00	0.90	3.00	0.73	3.00	0.65
F	0.06	48.0	3.00	3.33	0.85	3.33	0.67	3.43	0.63
G	0.09	32.5	2.60	2.87	0.94	2.86	0.86	2.86	0.82
I	0.12	30.1	2.61	2.65	0.95	2.65	0.88	2.67	0.83
M	0.02	32.2	1.80	1.88	0.87	1.88	0.74	1.88	0.70
P	0.20	31.7	3.00	3.03	0.96	3.00	0.89	3.00	0.86

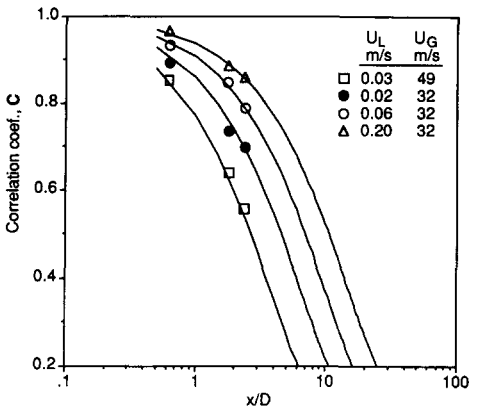

Figure 21. Correlation coefficient reduction with distance, indicative of fast deforming disturbance waves.

The evidence examined so far (dominant frequencies, visual observations) suggests that there is no appreciable variation of the wave celerity in the circumferential direction. However, the validity of this suggestion can be questioned if one takes into account that the mean film thickness varies drastically in the circumferential direction and that the wave celerity is influenced, in general, by the film thickness.

To further examine the motion of large waves and possibly to reconcile the above evidence, additional measurements of wave celerity were carried out by placing three probes at $\Theta = 0°$ and at relative distances $\Delta x = 3$, 9 and 12 cm on a new test section especially constructed for these experiments. The wave celerities were determined from the time delays, obtained from the respective cross-correlation functions. For each set of flow conditions, the three celerities were almost identical and practically equal to the previously measured values. Additionally, the correlation coefficients C in each case showed a fairly steep reduction with distance, as indicated in table 3. Considering that this reduction is evidence of a fast deforming wave, an exponential function, $C = \exp[-\alpha(x/D)]$, was fitted to the data (figure 21) in order to estimate the mean lifetime of disturbance waves. The results are very interesting, suggesting that these waves "survive" and travel a distance of the order of 20 pipe dia. Recalling that the wave celerity is 2–3 m/s, their lifetime appears to be only a fraction of a second! The fastest changing waves are those generated at low liquid and relatively high gas flow rates. This is reflected in the values of the coefficient α of the above exponential function.

By taking into account all the data analyzed so far, the following physical picture is emerging with regard to large disturbance waves:

> Waves created in the liquid and covering *initially* a considerable portion of the circumference, in the lower part of the pipe, move with a nearly uniform axial wave velocity (U_c) at an angle with respect to the direction of gravity. These waves tend to deform very rapidly covering distances of the order of 20 pipe dia and having mean lifetimes < 1 s. Thus, they resemble *pulses*, continuously developing and disappearing. With respect to the inception of the disturbance waves, nothing concrete can be said at this time. However, interpretation of visual observations and of detailed droplet flux measurements [reported by Paras & Karabelas (1991)] suggests that gas–liquid interface shearing and, in particular, *atomization* may play a major role in wave deformation. Finally, the very short lifetimes of the disturbance waves, combined with the significant wave celerities, provide an explanation as to why no substantial variation of the wave celerity was detected in the circumferential direction.

Acknowledgements—Financial support by the Commission of European Communities (Contract No. EN3G-0040-GR) and the General Secretariat for Research & Technology of Greece is gratefully acknowledged.

The authors also wish to thank Drs N. Andritsos and V. Bontozoglou for their helpful comments and suggestions.

REFERENCES

ANDERSON, R. J. & RUSSELL, T. W. F. 1970 Circumferential variation of interchange in horizontal annular two-phase flow. *Ind. Engng Chem. Fundam.* **9,** 340–344.

ANDRITSOS, N. 1986 Effect of pipe diameter and liquid viscosity on horizontal stratified flow. Ph.D. Thesis, Univ. of Illinois, Urbana.

BARNEA, D., SHOHAM, O., TAITEL, Y. & DUKLER, A. E., 1980 Flow pattern transition for gas–liquid flow in horizontal and inclined pipes. *Int. J. Multiphase Flow* **6,** 217–226.

BENDAT, J. S. & PIERSOL, A. G. 1971 *Random Data: Analysis and Measurement Procedures.* Wiley-Interscience, New York.

BUTTERWORTH, D. 1972 Air–water annular flow in a horizontal tube. *Prog. Heat Mass Transfer* **6,** 235–251.

BUTTERWORTH, D. & PULLING, D. J. 1973 RS95: Film flow and film thickness measurements for horizontal annular air–water flow. UKAEA Report No. AERE-R7576.

DALLMAN, J. C. 1978 Investigation of separated flow model in annular gas–liquid two-phase flows. PhD. Thesis, Univ. of Illinois, Urbana.

DARLING, R. S. & MCMANUS, H. N. 1968 Flow patterns in circular ducts with circumferential variation of roughness: a two-phase flow analog. In *Proc. 11th Midwestern Mechanics Conf.*, paper 9, pp. 153–163. Iowa State Univ. Press, Ames.

FISHER, S. A. & PEARCE, D. L. 1978 A theoretical model for describing horizontal annular flows. In *Two-phase Momentum, Heat and Mass Transfer in Chemical, Process and Energy Engineering Systems* (Edited by DURST, F., TSIKLAURI, G. V. & AFGAN, N.), pp. 327–333. Hemisphere/ McGraw-Hill, Washington, D.C.

FUKANO, T. & OUSAKA, A. 1989 Prediction of circumferential distribution of film thickness in horizontal and near-horizontal gas–liquid annular flow. *Int. J. Multiphase Flow* **15,** 403–420.

FUKANO, T., OUSAKA, A., MORIMOTO, T. & SEKOGUCHI, K. 1983 Air–water annular two-phase flow in a horizontal tube. 2nd Report. *Bull. JSME* **26,** 1387–1395.

JAMES, P. W., WILKES, N. S., CONKIE, W. & BURNS, A. 1987 Developments in the modelling of horizontal annular two-phase flow. *Int. J. Multiphase Flow* **13,** 173–198.

JAYANTI, S. & HEWITT, G. F. 1990 Structure of interfacial waves in air water horizontal annular flow. Presented at the *ICHMT Semin. on Phase-interface Phenomena in Multiphase Flow*, Dubrovnik, Yugoslavia.

KARAPANTSIOS, T. D., PARAS, S. V. & KARABELAS, A. J. 1989 Statistical characteristics of free falling films at high Reynolds numbers. *Int. J. Multiphase Flow* **15,** 1–21.

LAURINAT, J. E. 1982 Studies of the effects of pipe size on horizontal annular two-phase flows. Ph.D. Thesis, Univ. of Illinois, Urbana.

LAURINAT, J. E., HANRATTY, T. J. & DALLMAN, J. C. 1984 Pressure drop and film height measurements for annular gas–liquid flow. *Int. J. Multiphase Flow* **10,** 341–356.

LAURINAT, J. E., HANRATTY, T. J. & JEPSON, W. P. 1985 Film thickness distribution for gas–liquid annular flow in a horizontal pipe. *PhysicoChem. Hydrodynam.* **6,** 179–195.

LIN, P. Y. 1985 Flow regime transitions in horizontal gas–liquid flow. Ph.D. Thesis, Univ. of Illinois, Urbana.

LIN, T. F., JONES, O. C. LAHEY, R. G., BLOCK, R. C. & MAURASE, M. 1985 Film thickness measurements and modelling in horizontal annular flows. *PhysicoChem. Hydrodynam.* **6,** 197–206.

NENCINI, R. M. & ANDREUSSI, P. 1983 Study of the behavior of large disturbance waves in annular two-phase flow. *Can. J. Chem. Engng* **60,** 459–466.

PARAS, S. V. & KARABELAS, A. J. (1990) Wave characteristics of the liquid layer in horizontal annular flow. Presented at the *ICHMT Semin. on Phase-interface Phenomena in Multiphase Flow*, Dubrovnik, Yugoslavia.

PARAS, S. V. & KARABELAS, A. J. 1991 Droplet entrainment and deposition in horizontal annular flow. *Int. J. Multiphase Flow* **17,** 455–468.

PLETCHER, R. H. & MCMANUS, H. N. 1965 The fluid dynamics of 3-dimensional liquid films with free surface shear: a finite difference approach. In *Proc. 9th Midwestern Mechanics Conf.*, Madison, Wisc.

SCHADEL, S. A. 1988 Atomization and deposition rates in vertical annular two-phase flow. Ph.D. Thesis, Univ. of Illinois, Urbana.

SEKOGUCHI K., OUSAKA, A., FUKANO, T. & MORIMOTO, T. 1982 Air–water annular two-phase flow in a horizontal tube. 1st Report. *Bull. JSME* **25**, 1559–1566.

WILLIAMS, L. R. 1986 Entrainment measurements in a 4 inch horizontal pipe. M.Sc. Thesis, Univ. of Illinois, Urbana.